Do the Structures of Big ET-1 and Big ET-3 Adopt a Similar Overall Fold? Consequences for Endothelin Converting Enzyme Specificity†

N. B. Cronin and B. A. Wallace*

Department of Crystallography, Birkbeck College, University of London, Malet Street, London WC1E 7HX, U.K.

Received July 13, 1998; Revised Manuscript Received October 23, 1998

ABSTRACT: Big ET-1 and big ET-3 are precursor peptides which render endothelin-1 (ET-1) and endothelin-3 (ET-3) relatively unreactive and resistant to proteolytic cleavage. Big ET-1 is cleaved in vivo by ECE-1 (endothelin-converting enzyme), and big ET-3 is also cleaved but apparently to a significantly lesser extent by this enzyme. To shed light on the relation between structure and function, circular dichroism (CD) spectroscopy and homology modeling were used to determine whether big ET-1 and big ET-3 adopt similar secondary and tertiary structures. Analyses of the CD spectra and thermal denaturation indicate they have similar secondary structures and thermal stabilities. Superposition of the modeled coordinates of both peptides indicates that they can adopt the same overall fold except in the C-terminal residues, 34−38 in big ET-1 and 34−41 in big ET-3. This region corresponds to an area of complete sequence heterogeneity between the two peptides. A model has been developed which has a loop for residues 27−30 (HVVP in big ET-1), which have previously been demonstrated to be essential for eliciting efficient hydrolysis of the W21−V22 bond in big ET-1 and which have the sequence QTVP in big ET-3. Differences in affinity between big ET-1 and big ET-3 for ECE-1 thus appear to be due solely to sequence variations in the local region of the cleavage site.

The three-dimensional structure of endothelin-1 (*1*), a 21-amino acid polypeptide and the most potent naturally occurring vasoconstrictor yet discovered (*2*), has given us insight into its mode of binding to its heterotrimeric guanine nucleotide protein-coupled receptors (GPCR[1]), and it has been a target for the rational drug design of receptor antagonists. However, design of specific inhibitors has been difficult due to the existence of several receptor subtypes and the existence of three distinct endothelin isoforms. An alternative strategy for drug design is to inhibit the processing of the endothelin precursors to the active polypeptides.

Endothelin-1 (ET-1) is produced from an intermediate precursor big ET-1, a 38-amino acid polypeptide in humans, which performs a dual role in rendering ET-1 inactive while conferring resistance to proteolytic degradation. Evidence suggests that big ET-1 can act as a long-distance carrier of the biological activity of ET-1 in vivo (*3*). Endothelin-3 (ET-3) is protected in an analogous form in big ET-3, a 41-amino acid polypeptide. Big ET-1 and big ET-3 are produced from a zymogen, preproendothelin, by proteolysis at a pair of dibasic amino acids, one of the pair being proximal and one distal to the resultant big endothelin, by a member of the furin-like convertase family of Ca^{2+}-dependent serine proteases (*4*). The Trp21−Val22 bond of big ET-1 is then preferentially hydrolyzed by the homologous family of endothelin-converting enzymes (ECEs) (*5*, *6*). Both the endothelin-converting enzymes and the furin-like convertases are integral membrane proteins. Genetic evidence from the development of mouse embryos points to ECE-1 as a physiologically relevant endothelin-converting enzyme for both big ET-1 and big ET-3 in vivo (*3*). The three known isoforms of ECE-1, i.e., ECE-1a−c, derived from a single gene through the use of alternative promoters, have distinct tissue distributions and subcellular localizations and have equal affinity for big ET-1 and approximately 10% of this activity for big ET-3 in vitro (*7*). This was confirmed by Turner et al. (*8*), who found tissue-specific expression using antibodies raised against two ECE-1 rat isoforms in human umbilical vein endothelium cells (HUVEC) and transformed rat lung vascular endothelial cells (TRLEC-03). Another isoenzyme, ECE-2 with an acidic pH optimum and a isopeptide substrate selectivity similar to that of ECE-1, has been cloned from bovine adrenal cortex, but it is not known whether ECE-2 is expressed in humans (*9*). The processing site in big ET-3 has a Trp−Ile bond rather than the Trp−Val scissile bond found in both big ET-1 and big ET-2. Although there is a high degree of sequence homology between big ET-1, big ET-2, and big ET-3, a further variation between the endothelins occurs in residues 27−29 which have the sequence HVV in human big ET-1, QTA in human big ET-2, and QTV in human big ET-3 (Figure 1). While these latter sequence variations show a degree of conservation in physicochemical properties (*10*), the C-terminal sequence in big ET-3 from residue 35 to 41 bears no homology to that of either big ET-1 or big ET-2, which are homologous to each other in this region. This could indicate a tertiary

† This work was supported by British Heart Foundation Grant 95009 (to B.A.W.).

* Corresponding author. Telephone: 44-171-631-6857. Fax: 44-171-631-6803. E-mail: ubcg91c@ccs.bbk.ac.uk.

[1] Abbreviations: CD, circular dichroism; ET-1, endothelin-1; ET-3, endothelin-3; ECE-1, endothelin-converting enzyme-1; GPCR, G-protein coupled receptor; NDSB195, nondetergent sulphobetaine 195.

10.1021/bi981689b CCC: $18.00
Published on Web 01/22/1999

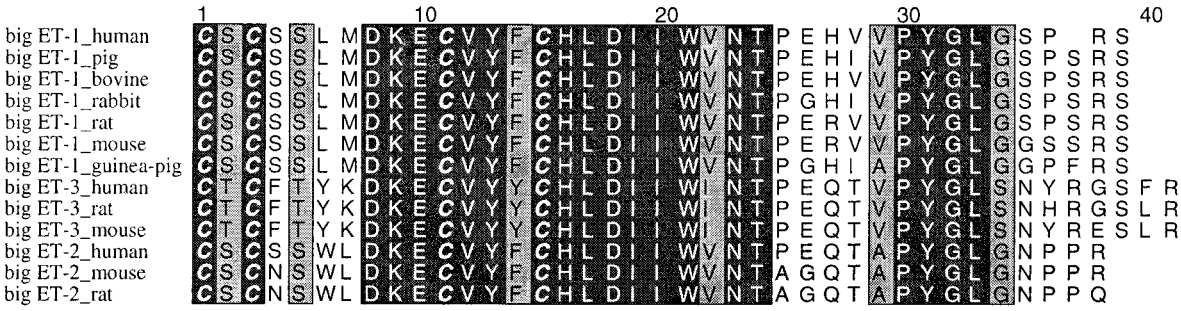

FIGURE 1: Sequence alignment of the currently known endothelin precursor (big ET) peptides shaded according to calculated conservation values (*10*), depicted using ALSCRIPT (*43*), with black indicating absolute sequence conservation and white nonhomologous substitution.

structural feature shared by big ET-1 and big ET-2 but not by big ET-3 in the C-terminal tail.

CD spectroscopy and homology modeling have been used in this study to examine whether big ET-1 and big ET-3 bear overall structural homology to each other and whether differences in susceptibility to proteolytic cleavage are due to overall differences in secondary and tertiary structure or due to local differences in the residues which bind in the specificity subsites of the enzyme. We have further examined whether a difference in thermal stability of the isoforms could account for any differences in proteolytic susceptibility.

EXPERIMENTAL PROCEDURES

Materials. Human big ET-1 and human big ET-3 were purchased from the Peptide Institute Inc. (Osaka, Japan). Solutions containing 0.2−0.5 mg/mL peptide in 0.1% acetic acid, 10 mM glycine buffer at pH 3.2, 10 mM Tris buffer at pH 8.5, or 10 mM sodium citrate buffer at pH 4.0, with or without 0.25 M NDSB195 (nondetergent sulfobetaine), were prepared. NDSB195 from Calbiochem-Novabiochem was used.

Circular Dichroism Spectroscopy. All measurements were performed with an AVIV 62ds spectropolarimeter using 0.5 mm path length cells. The instrument was calibrated for wavelength with benzene and for optical rotation with *d*-camphorsulfonic acid. In the wavelength mode, all data were collected over a wavelength range of 185−300 nm in 0.2 nm intervals, using a 1.5 nm bandwidth. For each sample, five scans of both peptide solutions and buffer alone were obtained and averaged. After the buffer baseline was subtracted, the net spectrum was smoothed using a Savitzky-Golay filter (*11*). The results are expressed as mean residue ellipticity. In the temperature mode, the thermally induced denaturation was performed by monitoring changes in the far-UV CD spectra at 205 nm, scanning from 20 to 100 °C, in 1 °C intervals with an equilibration time of 2.5 min at each point.

CD Analyses. Data points were analyzed at 0.2 nm intervals between 190 and 240 nm using a normalized constrained fitting procedure which required the fraction of each type of secondary structure to be positive and normalized the overall sum to unity (*12, 13*). The normalized root-mean-square deviation (NRMSD) parameter for each curve fitted was a measure of $[\sum_N(\theta_{exptl} - \theta_{calcd})^2/\sum_N(\theta_{exptl})^2]^{1/2}$, where θ_{exptl} and θ_{calcd} are the experimental and calculated mean residue ellipticities, respectively, and N was the number of data points used (*14*). Values of less than 0.1 are indicative of good correlation between the calculated and the actual secondary structural content of a protein (*15*). The reference data set used was a combination of the reference data set of Brahms and Brahms (*15*) and the data set of Chang et al. (*12*).

Molecular Modeling. Homologues were identified using the gonnet+predicted-secondary-structure method (*16*). Coordinates for the X-ray structures of scorpion toxin II (2sn3) and endothelin-1 (1edn) and the NMR structure of charybdotoxin (2crd) were obtained from the Brookhaven Protein Data Bank. Modeling was carried using the program MODELLER (*17*).

RESULTS AND DISCUSSION

Comparisons of the CD Spectra of Big ET-1 and Big ET-3. The CD spectra of big ET-1 and big ET-3 in 0.1% aqueous acetic acid (pH 4.0) are both characterized by broad minima at ∼206 nm (Figure 2a). The spectra are very similar except for an unusual positive band at ∼233 nm in the big ET-3 spectrum. Tyrosine side chains can give rise to a positive band at ∼228 nm [which in this case is slightly red-shifted by the strong negative contributions of the peptide groups (*18*)]. Such peaks are detectable even in the presence of the peptide backbone ellipticity if tyrosines comprise a significant proportion of the amino acid composition. This is the case for big ET-3, which has five tyrosines in contrast to big ET-1 which has only two, hence the spectral difference in this region.

Comparisons were made of big ET-1 and big ET-3 in the presence and absence of NDSB195 to ascertain whether NDSB195 has any effect on secondary structure. Big ET-3 is highly insoluble in water and in buffered solutions at pH 7.0 and is only sparingly soluble in lower- or higher-pH buffers. NDSB195 is a zwitterionic ammonium propane sulfonic derivative which ameliorates the solubility of proteins and prevents nonspecific aggregation with the advantage that this is not at the expense of denaturation (*19*). The CD spectrum of big ET-3 in 0.1% aqueous acetic acid (pH 4.0) and its spectrum in 10 mM sodium citrate (pH 4.0) containing 0.25 M NDSB195, a nondetergent sulfobetaine, are very similar (Figure 2b). Comparison of the spectrum of big ET-1 in 10 mM Tris (pH 8.5) containing 0.25 M NDSB195 with that of big ET-1 in aqueous acetic acid (pH 4.0) showed they were also similar (Figure 2c), the latter being virtually identical to previous data for big ET-1 at pH 6.0 and 7.0 (*20*). The spectrum at the higher pH with the nondetergent sulfobetaine is slightly blue-shifted, its minimum being at ∼205 nm instead of at ∼207 nm. This type of shift is commonly seen in the presence of nonaqueous solvent components (*26*).

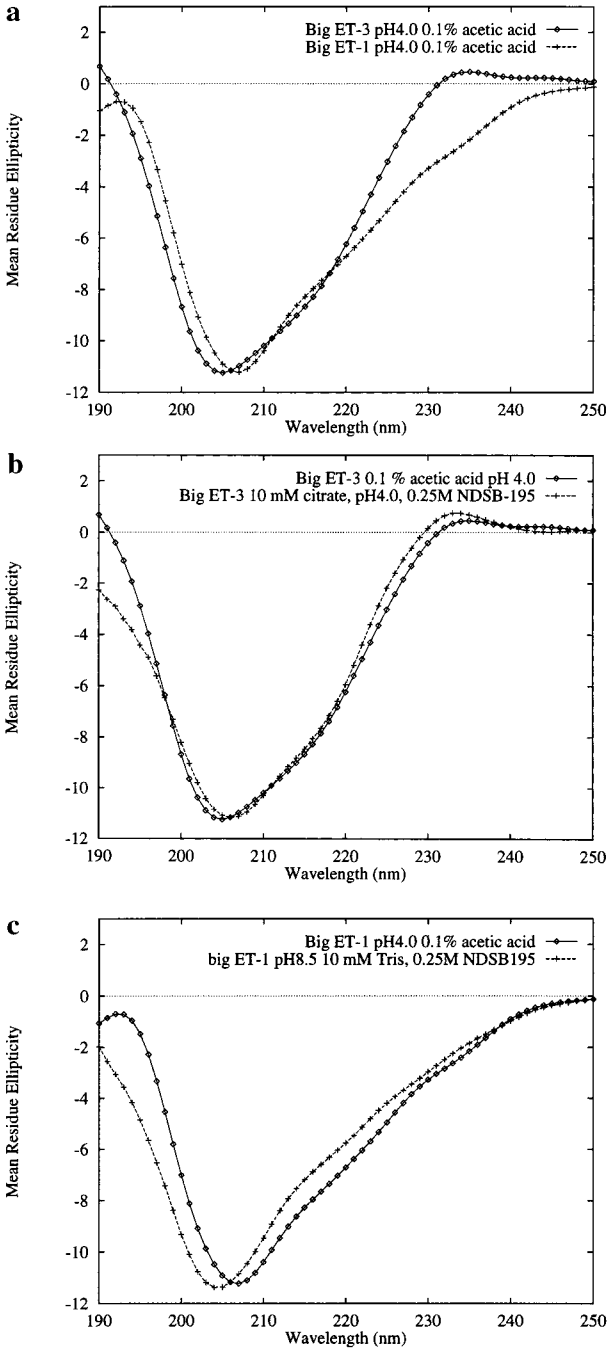

FIGURE 2: Circular dichroism spectra (a) of big ET-1 (+) and big ET-3 (◇) in 0.1% aqueous acetic acid at pH 4.0, (b) of big ET-3 in 0.1% aqueous acetic acid at pH 4.0 (◇) and big ET-3 in 10 mM citrate at pH 4.0 with 0.25 M NDSB195 (+), and (c) of big ET-1 (◇) at pH 4.0, as above, and in 10 mM Tris buffer at pH 8.5 with 0.25 M NDSB195 (+).

Estimation of Secondary Structure and pH Effects. Analyses of the CD spectra of oligopeptides by empirical methods for estimating their secondary structural composition are less reliable when compared to similar analyses of protein structures, due to the highly flexible nature of peptides in solution, where they can adopt multiple conformations which are often solvent-dependent or pH-dependent (*20*). The crystal structure of ET-1 indicates that it contains an irregular helix stretching from residue 9 to 21 (*1*). Previous NMR studies of ET-1 in nonphysiological solvents also indicated helical stretches which involved fewer residues, implying that the stability of the helix depends on the environment of the peptide (*21*). The structure of ET-3 in 10% aqueous acetic acid determined by NMR (*22*) suggested an irregular helix for residues 9−15. This result is consistent with the NMR study of ET-3 at pH 3.6 by Mill et al. (*23*), which inferred an irregular helix for the same residues. CD and NMR analyses of an analogous polypeptide sarafotoxin-6b (S6b) in aqueous solution (*24*) found no difference in its CD spectra at pH 7.4 and 3.6, and the study revealed a regular right-handed α-helix extending from residue 9 to 17.

Table 1: Comparison of Calculated Secondary Structures for Big ET-1 and Big ET-3[a]

sample	pH	α (%)	β (%)	t (%)	c (%)	NRMSD
big ET-1	4.0[b]	1	45	6	49	0.05
big ET-3	4.0[b]	0	45	5	50	0.07
big ET-3	4.0[c]	0	45	3	52	0.09
big ET-1	8.5[d]	2	40	6	51	0.05

[a] α, α-helix content; β, β-sheet content; t, β-turn content; c, coil content; NRMSD, normalized root-mean-square deviation. [b] Big ET-1 and big ET-3 in 0.1% acetic acid at pH 4.0. [c] Big ET-3 in 10 mM sodium citrate at pH 4.0 with 0.25 M NDSB195. [d] Big ET-1 in 10 mM Tris at pH 8.5 with 0.25 M NDSB195.

The calculated secondary structures for big ET-1 and big ET-3 (Table 1) are similar to the secondary structure previously determined for big ET-1 at pH 7.0 by CD spectroscopy (*20*). Because the helix found in the X-ray and NMR structures of ET-1 is disordered, i.e., with φ and ψ angles outside the expected region for helix in the Ramachandran plot, the low helix but high coil content is expected. The reference data set used was a combination of the reference data sets of Brahms and Brahms (*15*) and Chang et al. (*12*) as this gave the best fit and most consistent NRMSD parameters and is thus the most likely representation of the types of secondary structure present in these peptides. The relative proportions of α-helix, β-sheet, and β-turn are virtually identical for big ET-1 and big ET-3 in 0.1% aqueous acetic acid (Table 1). Similarly, big ET-3 in 0.1% aqueous acetic acid and in sodium citrate, both at pH 4.0, but with the latter containing NDSB195, are also essentially the same (Table 1), indicating the absence of any significant effect of this solubilizing agent on the secondary structure. For big ET-1, the calculated secondary structures at pH 4.0 and 8.5 with NDSB195 indicate only a very slight increase of helical and coil content at the higher pH with a small decrease of β-sheet content but no change in β-turn content.

Temperature-Induced Conformational Transitions. The thermally induced denaturations of the secondary structures of big ET-1 at pH 3.2 and at pH 8.5 with NDSB195 and of big ET-3 at pH 3.2 in 10 mM glycine buffer and at pH 4.0 in 10 mM sodium citrate with NDSB195 were monitored as an increase in ellipticity of the CD peak at 205 nm. Big ET-1 in 10 mM glycine buffer at pH 3.2 exhibits a gradual and continuous increase in ellipticity (corresponding to a loss of secondary structure) rather than an abrupt cooperative pattern of unfolding between 20 and 100 °C. Even at 100 °C, there is still a considerable amount of residual secondary structure (Figure 3a). For big ET-3 in 10 mM glycine at pH 3.2, there is a similar gradual and monotonic increase in ellipticity at 205 nm between 20 and 100 °C with a gradient (change in ellipticity per degree Celsius), suggestively similar to that of big ET-1. For big ET-1 in 10 mM Tris (pH 8.5) and 0.25 M NDSB195, denaturation occurs with a sharp transition

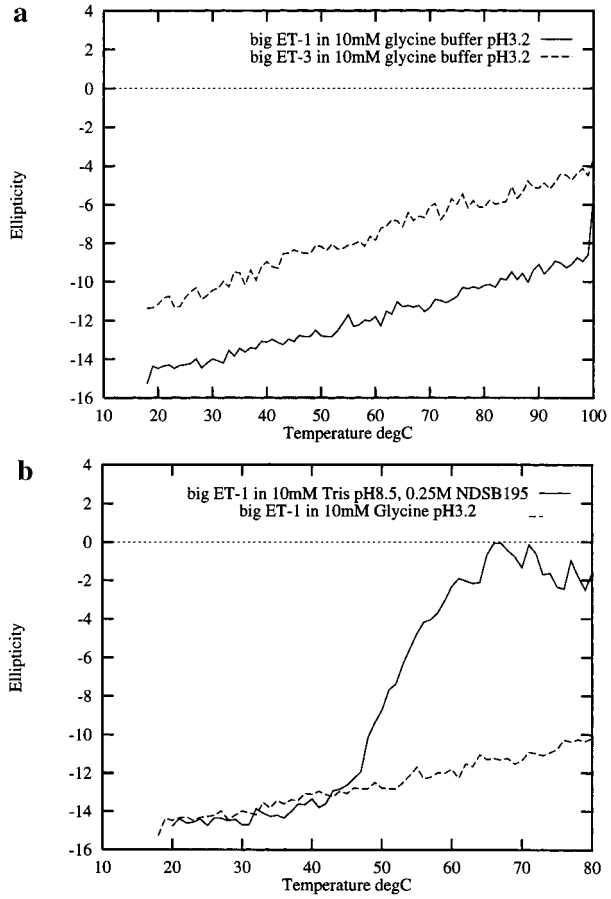

FIGURE 3: Comparison of the changes in ellipticity at 205 nm with temperature of (a) big ET-1 (−) and big ET-3 (- -) in 10 mM glycine buffer at pH 3.2 and (b) big ET-1 in 10 mM Tris buffer at pH 8.5 with 0.25 M NDSB195 (−) and in 10 mM glycine at pH 3.2 (- -).

from the signal of the native peptide to that of the denatured form (i.e., from an ellipticity θ of −15 mdeg to one of 0 mdeg) between 45 and 60 °C (Figure 3b). Big ET-3 in 10 mM sodium citrate buffer (pH 4.0) and 0.25 M NDSB195 exhibits no loss of signal between 20 and 80 °C, i.e., a temperature-independent part, and then a gradual loss of secondary structure between 80 and 100 °C, indicative of a broad thermal unfolding transition (data not shown).

The temperature-induced denaturation gradients of big ET-1 and big ET-3 at pH 3.2 are virtually identical, which is consistent with them having similar secondary and possibly tertiary structures and similar thermal stabilities. However, there is a significant pH effect on the temperature-induced denaturation patterns of both big ET-1 and big ET-3, which may imply a pH effect on their tertiary structures. The secondary structures of big ET-1 at pH 3.2 and 8.5 at room temperature are very similar, but the denaturation profiles differ. The thermally induced cooperative unfolding transition at pH 8.5, which is characteristic of native-type structure particularly in small single-domain proteins, is disrupted at pH 3.2 with a profile characteristic of compact denatured or stable "molten globule" states of many proteins. The acid treatment of proteins has been observed to produce compact intermediate states that retain significant secondary structure and compactness due to the presence of a hydrophobic core and a tertiary structure reminiscent of the native fold but with altered interactions and packing (*25*). Such structures are less unfolded than those obtained with high concentrations of chaotropic agents such as guanidine hydrochloride or urea (*27*, *28*). This has been hypothesized to result from electrostatic repulsion which disrupts the native structure but fails to completely overcome the interactions favoring tertiary folding such as hydrophobic forces, disulfide bonds, and salt bridges The stability of compact intermediate states as evidenced here for both big ET-1 and big ET-3 at pH 3.2 has been demonstrated to result from the binding of anions to basic charged groups as the protein unfolds, thus masking repulsive positive charge and allowing intrinsic hydrophobic forces to cause collapse to a compact state (*27*). At pH 8.5, the sharp cooperative transition from the initial folded to the final unfolded state indicates that intermediate states are energetically unfavorable and not stabilized at this pH.

Comparison of Big ET-1 and Big ET-3 by Homology Modeling. Modeling of big ET-1 and big ET-3 was based on homology with scorpion toxin II (*29*) whose sequence is 27% homologous with that of big ET-1. The alignment was produced using the gonnet+predicted-secondary-structure method of Fischer and Eisenberg (*16*). The X-ray structure of ET-1 (*1*) and the NMR structure of charybdotoxin (*30*) were also included in the modeling of the N-terminal regions of the ET precursors. The many different NMR structures of ET-1 (see ref *31* for a comparison between them and the X-ray structure) and ET-3 were not included in the modeling strategy since their C-terminal residues (15−21) are poorly defined and highly variable among these structures and, more significantly, the low pH [e.g., pH 3.2 (*32*)] of these experiments appears to give rise to populations of partially unfolded structures. Moreover, SAR studies have suggested that the X-ray structure which was from a simple aqueous solution but none of the NMR structures (principally from solutions incorporating high levels of organic solvents) is likely to be the biologically relevant form of the molecule (*33*). The program MODELLER (*17*) was used to initially calculate distance and dihedral angle restraints as conditional probability density functions on the target sequence from its alignment with template three-dimensional structures. The model was refined using molecular dynamics with simulated annealing.

The models obtained for both big ET-1 and big ET-3 predict identical structures for both for the region including residues 1−34. Superposition of the two structures shows a divergence of conformation from residue 34 to 38 in big ET-1 and residue 34 to 41 in big ET-3 (Figure 4). This is, in fact, a continuous region of the alignment where residues are unconserved across all sequences coupled with gaps and a number of species differences among the isoforms (Figure 1). Two previous modeling studies of big ET-1, based on either a threading algorithm (*34*) or homology modeling techniques (*35*), gave rise to structures which differed somewhat both from each other and from the structure of big ET-1 predicted here; no previous structure has previously been produced for big ET-3. The current models predict disulfide bridges between residues 1−15 and 3−11, an irregular helix comprising residues 8−16, extended β-strands involving residues 1−4, 21−26, and 31 and 32, and β-turns at residues 4−7, 17−20, and 27−30 (33−36 and 35−38 in the C terminus of big ET-1 and 36−39 in the C terminus of big ET-3). Residues Trp21 and Ile22 (big ET-3) or Trp21 and Val22 (big ET-1) of the scissile bond adopt a gauche (+) conformation for the χ_1 side chain torsion angle in both

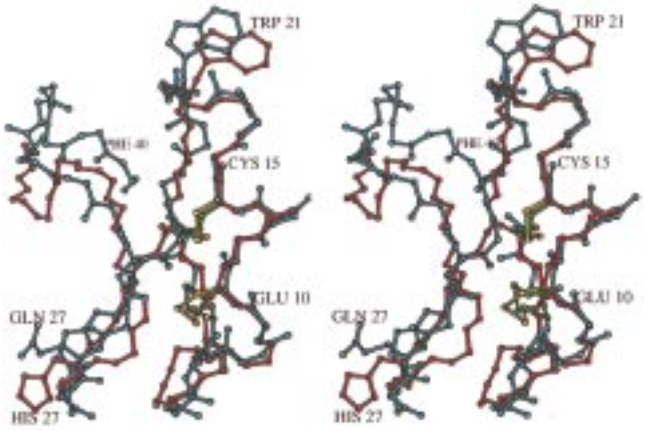

FIGURE 4: Stereoview of the superposition of modeled coordinates for big ET-1 (red) and big ET-3 (blue). The backbone atoms for all residues and side chain atoms of residues 21 and 27 are shown. The structures were based on homology modeling with the X-ray structures of ET-1 (1edn) (*1*), scorpion toxin II (2sn3) (*29*), and the NMR structure of charybdotoxin (2crd) (*30*) displayed using BOBSCRIPT (*44*).

models and have β-strand main chain conformations which would facilitate the possibility of this molecule binding in an extended fashion in the active side of ECE with side chains occupying specificity subsites on either side of the scissile bond. NMR solution studies (*36*) of big ET-1 indicate that the tail region (L17−S38) undergoes faster internal and independent motion compared to the core region (C1−H16) and showed that the tail region (L17−S38) exhibits a great deal of flexibility under the conditions used in the spectroscopic measurements.

The relevant features of the model structures produced in this study to the experimental data are that they predict a similar fold for both big ET-1 and big ET-3 which corroborates the CD analysis. Hydrolysis rates of substituted analogues of big ET-1 indicate that ECE recognizes the sequence from H27 to G34 in the C terminus (*37*, *38*) as well as the scissile dipeptide, and thus, the mode of recognition by ECE is quite unique, since a related enzyme, neutral endopeptidase 24.11 (NEP), recognizes only the hydrophobic amino acid residues at the processing site (*39*).

The current model has a loop comprising residues 27−30 (HVVP in big ET-1 and QTVP in big ET-3) which may form an interface with a hydrophobic surface in ECE. Intuitively, the difference at residue 27 between His in big ET-1 and Gln in big ET-3 may reflect different pH optima for hydrolysis of big ET-1 and big ET-3, suggesting that big-ET-3 may be cleaved intracellularly in vivo. Although ET-3 is present in the plasma its provenance is unclear since, in contrast to big ET-1, it is not released by endothelial cells. Also, neither intact nor permeabilized human umbilical vein endothelial cells were found to process big ET-3, while intact human umbilical vein smooth muscle cells did process big ET-3 (*40*). A possible source is the adrenal gland, in which immunoreactive big ET-3 has been detected in secretory cells of the medulla (*41*).

Knowledge of the similarities and differences between the tertiary folds of big ET-1 and big ET-3 is important for understanding the specificity of ECE and the bound conformations of the big ET peptides for drug design for inhibitors of the ECE enzymes. Given the likelihood that ET-1 and ET-3 are produced by different isoforms of ECE, designing selective inhibitors of these isoforms could potentially allow unique inhibition of specific functionalities of both peptides. The potential for specific inhibition is further enhanced by the observation that 95% of the total expressed ECE-1b is intracellular (*7*) while ECE-1a and ECE-1c are present on the cell surface, and thus, there exists the potential for tailoring specific drugs which can or cannot cross the cell membrane.

Our current understanding of ECE-1 specificity arises from the development of a series of truncated or elongated N-terminal and C-terminal fragments of preproendothelin-1 and big ET-1. By mutation of the pair of dibasic consensus sequences for the furin-like convertase in preproendothelin-1, it was demonstrated that cleavage at the N-terminal sequence is not required for subsequent cleavage by ECE-1 but cleavage at the C-terminal sequence is critical for further processing by ECE-1. However, mutations at both dibasic consensus sequences blocked the formation of active ET-1 (*4*). Furthermore, big ET-1 was cleaved by ECE-1 after deletion of 15 N-terminal amino acid residues (*37*). In addition, it was established that the N-terminal disulfide loop structure in big ET-1 compromises the activity of ECE-1 since big ET-1 (residues 16−37) shows 3-fold enhanced activity relative to the native big ET-1 peptide (*37*). Specifically, big ET-1 residues 18−34 are necessary and sufficient for optimal activity of ECE-1 (*42*). Of this fragment, residues 18−21, 23−26, and 30−33 are identical in human big ET-1 and human big ET-3, i.e., 75% sequence identity (Figure 1). On this basis alone, it is highly probable that the overall folds of the two isoforms are similar, and this was borne out by the present CD analyses.

ACKNOWLEDGMENT

We thank H. Peto for helpful discussions and suggestions.

REFERENCES

1. Janes, R. W., Peapus, D. H., and Wallace, B. A. (1994) *Nat. Struct. Biol. 1*, 311−319.
2. Yanagisawa, M., Kurihara, H., Kimura, S., Tomobe, Y., Kobayashi, M., Mitsui, Y., Yazake, Y., Goto, K., and Masaki, T. (1988) *Nature 332*, 411−415.
3. Yanagisawa, H., Yanagisawa, M., Kapur, R. P., Richardson, J. A., Williams, S. C., Clouthier, D. E., de Wit, D., Emoto, N., and Hammer, R. E. (1998) *Development 125*, 825−836.
4. Kido, T., Sawamura, T., Hoshikawa, H., D'Orleans-Juste, P., Denault, J. B., Leduc, R., Kimura, J., and Masaki, T. (1997) *Eur. J. Biochem. 244*, 520−526.
5. Fabrini, S. F., Vitale, A., Pedrazzini, E., Nitti, G., Zamai, M., Tamburin, M., Caiofla, V. R., Patrono, C., and Benatti, L. (1993) *Proc. Natl. Acad. Sci. U.S.A. 90*, 3923−3927.
6. Corder, R. (1996) *Biochem. Pharmacol. 51*, 249−266.
7. Schweizer, A., Valdenaire, O., Nelbock, P., Deuschle, U., Dumas-Milne-Edwards, J.-B., Stumpf, J. G., and Loffler, B.-M. (1997) *Biochem. J. 328*, 871−877.
8. Brown, C. D., Barnes, K., and Turner, A. J. (1998) *FEBS Lett. 424*, 183−187.
9. Emoto, N., and Yanagisawa, M. (1995) *J. Biol. Chem. 25*, 15262−15268.
10. Livingstone, C. D., and Barton, G. J. (1993) *Comput. Appl. Biosci. 9*, 745−756.
11. Savitzky, A., and Golay, M. J. E. (1964) *Anal. Chem. 36*, 1627−1639.

12. Chang, C. T., Wu, C.-S. C., and Yang, J. T. (1978) *Anal. Biochem. 91*, 13−31.
13. Wallace, B. A., and Teeters, C. L. (1987) *Biochemistry 26*, 65−70.
14. Mao, D., Wachter, E., and Wallace, B. A. (1982) *Biochemistry 21*, 4960−4968.
15. Brahms, S., and Brahms, J. (1980) *J. Mol. Biol. 138*, 149−178.
16. Fischer, D., and Eisenberg, D. (1996) *Protein Sci. 5*, 947−955.
17. Šali, A., and Blundell, T. L. (1993) *J. Mol. Biol. 234*, 799−815.
18. Woody, R. W. (1978) *Biopolymers 17*, 1451−1467.
19. Vuillard, L., Baalbaki, B., Lehmann, M., Nørager, S., Legrand, P., and Roth, M. (1996) *J. Cryst. Growth 168*, 150−154.
20. Wallace, B. A., and Corder, R. (1997) *J. Pept. Res. 49*, 331−335.
21. Saudek, V., Hoflack, J., and Pelton, J. T. (1991) *Int. J. Pept. Protein Res. 37*, 174−179.
22. Bortmann, P., Hoflack, J., Pelton, J. T., and Saudek, V. (1991) *Neurochem. Int. 18*, 491−496.
23. Mills, R. G., O'Donoghue, S. I., Smith, R., and King, G. F. (1992) *Biochemistry 31*, 5640−5645.
24. Mills, R. G., Atkins, A. R., Harvey, T., Junius, F. K., Smith, R., and King, G. F. (1991) *FEBS Lett. 282*, 247−252.
25. Xie, D., and Freire, E. (1994) *Proteins: Struct., Funct., Genet. 19*, 291−301.
26. Chen, Y., and Wallace, B. A. (1997) *Biophys. Chem. 65*, 65−74.
27. Fink, A. L., Calciano, L. J., Goto, Y., Kurotsu, T., and Palleros, D. R. (1994) *Biochemistry 33*, 12504−12511.
28. Kolvenbach, C. G., Narhi, L. O., Philo, J. S., Li, T., Zhang, M., and Arakawa, T. (1997) *J. Pept. Res. 50*, 310−318.
29. Zhao, B. G., Carson, M., Ealick, S. E., and Bugg, C. E. (1992) *J. Mol. Biol. 227*, 239−252.
30. Bontems, F., Gilquin, B., Roumestand, C., Menez, A., and Toma, F. (1992) *Biochemistry 31*, 7756−7764.
31. Wallace, B. A., Janes, R. W., Bassolino, D. A., and Krystek, S. R., Jr. (1995) *Protein Sci. 4*, 75−83.
32. Andersen, N. H., Chen, C., Marschner, T. M., Krystek, S. R., Jr., and Bassolino, D. A. (1992*) Biochemistry 31*, 1280−1295.
33. Wallace, B. A., and Janes, R. W. (1995) *J. Cardiovasc. Pharmacol. 26*, S250−S253.
34. Peto, H., Corder, R., Janes, R. W., and Wallace, B. A. (1996) *FEBS Lett. 394*, 191−195.
35. Menziani, M. C., Cocchi, M., De Benedetti, P. G., Gilbert, R. G., Richards, W. G., Zamai, M., and Caiolfa, V. R. (1991) *J. Chim. Phys. 88*, 2687−2694.
36. Inooka, H., Endo, S., Kikuchi, T., Waldmasu, M., Mizuta, E., and Fujino, M. (1990) *Pept. Chem. 28*, 409−413.
37. Okada, K., Arai, U., Hata, M., Matsuyama, K., and Yano, M. (1993) *Eur. J. Biochem. 218*, 493−498.
38. Ohnaka, K., Takayangi, R., Nishikawa, M., Haji, M., and Nawata, H. (1993) *J. Biol. Chem. 268*, 26749−26766.
39. Liu, W., Takayanagi, R., Ito, T., Oba, K., and Nawata, H. (1997) *FEBS Lett. 420*, 103−106.
40. Davenport, A. P., Kuc, R. E., and Mockridge, J. W. (1998) *J. Cardiovasc. Pharmacol. 31*, S1−S3.
41. Davenport, A. P., Hoskins, S. L., Kuc, R. E., and Plumpton, C. (1996) *Histochem. J. 28*, 779−790.
42. Turner, A. J., and Murphy, L. J. (1996) *Biochem. Pharmacol. 51*, 91−102.
43. Barton, G. J. (1993) *Protein Eng. 6*, 37−40.
44. Esnouf, R. M. (1997*) J. Mol. Graphics Modell. 15*, 132−134.

BI981689B